Quantum wires in multidimensional microcavities: Effects of photon dimensionality on emission properties

C. Constantin, E. Martinet, D. Y. Oberli, and E. Kapon
Institute of Quantum Electronics and Photonics, Swiss Federal Institute of Technology-EPFL, 1015 Lausanne, Switzerland

B. Gayral and J. M. Gérard
CNRS/Laboratoire de Photonique et de Nanostructures, Boîte Postale 29, 92222 Bagneux Cedex, France
(Received 25 September 2001; revised manuscript received 4 February 2002; published 3 October 2002)

Seeded self-ordered, strained, 10-nm-size $In_{0.15}Ga_{0.85}As/GaAs$ V-groove quantum wires (QWR's) have been incorporated into multidimensional, high finesse ($Q \sim 5000$), micron-size $AlAs/Al_{0.07}Ga_{0.93}As$ photon-well, photon-wire (PWR), and photon-dot (PD) Bragg-air microcavities. The impact of the photon dimensionality on the QWR spontaneous emission is systematically elucidated in the spectral, spatial, temporal, and polarization domains using different microphotoluminescence techniques. Larger effects are demonstrated for resonant cavities confining in multiple dimensions and of smaller sizes. We observe increasingly rich structuring of the emission spectra and patterns for decreasing cavity dimensionality, leading to a series of sharp (0.28 meV) lines with enhanced intensities ($\times 50$) at specific directions in fully confined PD's. Photon lateral confinement in PWR's and PD's is necessary to evidence cavity-induced polarization effects and a spontaneous emission rate enhancement by a Purcell factor of $\times 1.7$, limited by the QWR inhomogeneous broadening. The results are interpreted in terms of the redistribution of the QWR emission into confinement-induced resonances in the photon mode distribution in the different cavities. In particular, systematic wave-vector quantization in the directions of photon confinement, and dispersive behavior in the free propagation directions are evidenced in close agreement with model calculations.

DOI: 10.1103/PhysRevB.66.165306 PACS number(s): 81.15.Gh, 42.60.Da, 71.35.Gg

I. INTRODUCTION

Optical semiconductor structures are becoming increasingly important as model systems for investigating the light-matter interaction, as well as key optoelectronic components for modern information technologies. A substantial body of work has been dedicated to the control of the carrier and photon states in such structures, using confinement and dimensionality effects to engineer their interaction and to tailor the optical properties for improved device performances.[1,2]

The confinement of the charge carriers in multiple directions has been widely exploited in quantum nanostructures[3] termed two-dimensional quantum wells (2D QW's), 1D quantum wires (QWR's), and 0D quantum dots (QD's). In particular, laterally confined QWR's and QD's have attracted considerable attention owing to their unique properties (see Refs. 4–6). Theoretical predictions for QWR's include a strongly peaked, singular, free-carrier density of states (DOS) leading to sharper optical transitions, narrower spectral gain,[7] and enhanced optical nonlinearities.[8] Moreover, strong valence-subband mixing at the center of the Brillouin-zone results in intrinsic optical polarization anisotropy.[9] Furthermore, the increasing role of Coulomb correlations up to high carrier densities[10] is evidenced by a larger exciton binding energy,[11] and a redistribution of the oscillator strength that suppresses the singularity in the joint DOS at the band edge in favor of excitonic transitions.[12,10] The fabrication of laterally confined QWR's however still represents a challenging technological task. Among the different fabrication techniques implemented, only few have met with the stringent structural requirements faced.[4,5] Among these, seeded self-ordered QWR's grown on V-grooved substrates have shown unambiguous 1D features,[13,14] thanks to their uniformity, which is a direct result of the strong driving force towards self-organization during their formation.[15]

The introduction of additional photon confinement obtained by embedding the nanostructures in optical microcavities or photonic crystals has burgeoned into a major avenue for tailoring the optical properties of semiconductors.[1,16,17] In fact, the *simultaneous* control of the carrier and photon states with quantum size and dimensionality effects allows to drastically modify spontaneous emission (SE) characteristics in the weak-coupling regime.[1,16] Hence, a sharpening of the emission spectra, an increased directionality of the emission pattern, an enhancement of the emission rate, and an anisotropy of the emission polarization are predicted in such confined systems. Increasing control over the SE process is expected when decreasing the photonic dimensionality in 2D photon wells (PW's), 1D photon wires (PWR's), and 0D photon dots (PD's). Therefore, the fields of confined electrons and confined photons are pursuing a parallel trend with a systematic reduction in the structure size and dimensionality, ultimately aiming at the manipulation of a single-carrier state and a single-cavity mode. Weakly coupled systems combining nanostructures and microcavities of various dimensionalities have been fabricated, exhibiting various degrees of SE control. The ease of fabrication of QW's has allowed their early incorporation in multidimensional microcavities and the demonstration of the above principles. In the weak-coupling regime, drastic changes in the SE spectrum and pattern were obtained by inserting the QW's in PW's,[18,19] whereas lateral photon confinement in PWR's (Ref. 20) and PD's (Refs. 21 and 22) was necessary to significantly alter the SE polarization and rate. In the strong-

coupling regime, polaritonic dispersions have been measured for QW's in PW's,[23] PWR's,[24] and PD's.[25] QD's have been incorporated in PW's,[26] and in PD's of various geometry,[27–29] as a realization of the ultimate coupled 0D system, allowing for significant enhancement ($\times 5$[30] to $\times 18$[28]) of the SE rate.

In contrast, few experimental studies[31,32] deal with the intermediate case of QWR's in microcavities, due to major fabrication difficulties. Such systems are quite interesting, however, as several specific predictions have been made for this intermediate case. In particular, the intrinsic optical anisotropy of QWR's provides for a polarization selection mechanism, leading to a larger SE coupling factor in vertical cavity surface emitting lasers.[33] Moreover, a short periodicity grating of QWR's inside a PW introduces additional interwire coupling resulting in marked effects in the emission properties,[34,35] which allows to control the main light output direction, therefore easing both lateral and vertical integration at the system level. Exciton-polaritons in a cylindrical microcavity where a QWR is embedded have also been theoretically studied.[36] Nonradiative damping, e.g., phonon broadening or inhomogeneous broadening, was included in this model and its effect on the existence of a vacuum field Rabi splitting in the absorption spectrum was analyzed: for broadening comparable to the Rabi splitting, the optical spectra were characterized by a single broad peak.

Recently, we reported on state-of-the-art strained InGaAs/GaAs V-QWR's exhibiting specific geometry, composition, and strain distribution.[37,38] Unambiguous 1D features were demonstrated in optical spectroscopy thanks to the strong carrier confinement.[14,37] Moreover, we succeeded in incorporating similar InGaAs/GaAs V-QWR's in high finesse, wavelength-size planar Bragg microcavities.[39] Preliminary observations of the resonant coupling between the 1D carrier and the 2D photon states in optical spectra were published in a previous Rapid Communication.[40] In the present paper, we report on the systematic investigation of the coupling between 1D carriers and 2D, 1D, 0D photon states in the spectral, spatial, temporal, and polarization domains using photoluminescence (PL) spectroscopy. Such coupling has been obtained by inserting the InGaAs QWR's in multidimensional Bragg-air microcavities, i.e., PW's, PWR's and PD's, respectively. As a result of the fairly large inhomogeneous broadening of the QWR's, the coupling of 1D excitons and the photon modes of the microcavities corresponds to the weak-coupling limit and no Rabi splitting is observed. We demonstrate larger modifications of optical properties for microcavities confining in more dimensions and of smaller sizes.

The paper is organized as follows. In Sec. II we briefly describe the fabrication process of InGaAs/GaAs V-QWR's in multidimensional Bragg-air microcavities and provide electron microscopy micrographs to evidence the high structural quality achieved. In Sec. III we demonstrate the one dimensionality of the V-QWR's using a combination of PL and PL excitation spectroscopy. In Sec. IV we elucidate the impact of the photon confinement on the QWR emission properties using a combination of energy-, angle-, time-, and polarization-resolved micro-PL (μPL) techniques. The increasing structuring complexity of the emission spectra for decreasing cavity dimensionality is presented in Sec. IV B, leading to the observation of single-photon modes in 0D PD's of different lateral size. The related increasing structuring of the far field pattern is studied using a charge-coupled device (CCD) camera for imaging in Sec. IV C, with the observation of images characteristic of the photon dimensionality. In Sec. IV D, we deduce a larger enhancement of the SE rate for cavities confined in multiple dimensions and of smaller sizes. PD structures are also used as a passive tool for getting insight into the diffusion of the hot QWR carriers. We compare in Sec. IV E the polarization properties of the QWR's in the various cavities. We finally summarize our results and conclude in Sec. V.

II. STRUCTURE OF QUANTUM WIRES IN MULTIDIMENSIONAL MICROCAVITIES

Our structures were fabricated using a combination of epitaxial growth and lithographic processes. The growth, using low-pressure organometallic chemical vapor deposition of InGaAs/GaAs heterostructures on V-grooved substrates, has been investigated and optimized in order to incorporate seeded self-ordered, lattice-mismatched V-QWR's in multidimensional Bragg-air microcavities using the following four-stage process.[39,41] First, a 25-pair $\lambda/4$ $AlAs/Al_{0.07}Ga_{0.93}As$ bottom Bragg mirror with a $\sim$120-nm-thick GaAs cap layer was grown at $T_s = 750\,^{\circ}C$ on a (100) GaAs substrate. The sample was then removed from the growth reactor and the cap layer patterned with a $[01\bar{1}]$-oriented V-groove array of short periodicity $\Lambda = 0.25\ \mu$m, using holographic photolithography and wet chemical etching. During a second growth step, the structure was completed with a $\lambda \sim 0.25\ \mu$m GaAs spacer with embedded $\sim$10-nm-thick $In_{0.15}Ga_{0.85}As/GaAs$ QWR's and a 20-pair $\lambda/4$ $AlAs/Al_{0.07}Ga_{0.93}As$ top Bragg mirror, thus yielding an array of QWR's in a PW. Note that the growth of the spacer and QWR's was performed at a reduced temperature of 550 °C, in order to obtain narrow QWR's and a fast planarization of the grating.[39] Finally, further reduction of the photon dimensionality was obtained by patterning the planar cavity with $\sim$micron-wide pillarlike and ridgelike structures using *e*-beam lithography and reactive ion etching (RIE),[41] thus yielding an array of QWR's in a PWR or in a PD.

The high structural quality and the size compatible with electron and photon confinement achieved in the fabricated structures is evidenced by the transmission electron microscopy (TEM) and scanning electron microscopy (SEM) images in Fig. 1. In (a) we show a typical dark-field TEM micrograph of a dense lateral array of $In_{0.15}Ga_{0.85}As/GaAs$ QWR's connected by near-{111}*A* side QW's and (100) top QW's (*s*-QW's and *t*-QW's). The crescent-shaped QWR's exhibit a vertical thickness at the center of 11 nm and a lateral width of 19 nm, with a uniformity better than 5% between wires. They possess defect-free interfaces thanks to their *in situ* fabrication scheme. A characteristic In enrichment in the center of the wires results in the darker contrast in the TEM image.[42] An In content larger than 0.2 in the core of the wire, in contrast to a value of 0.1 in the *s*-QW's, has

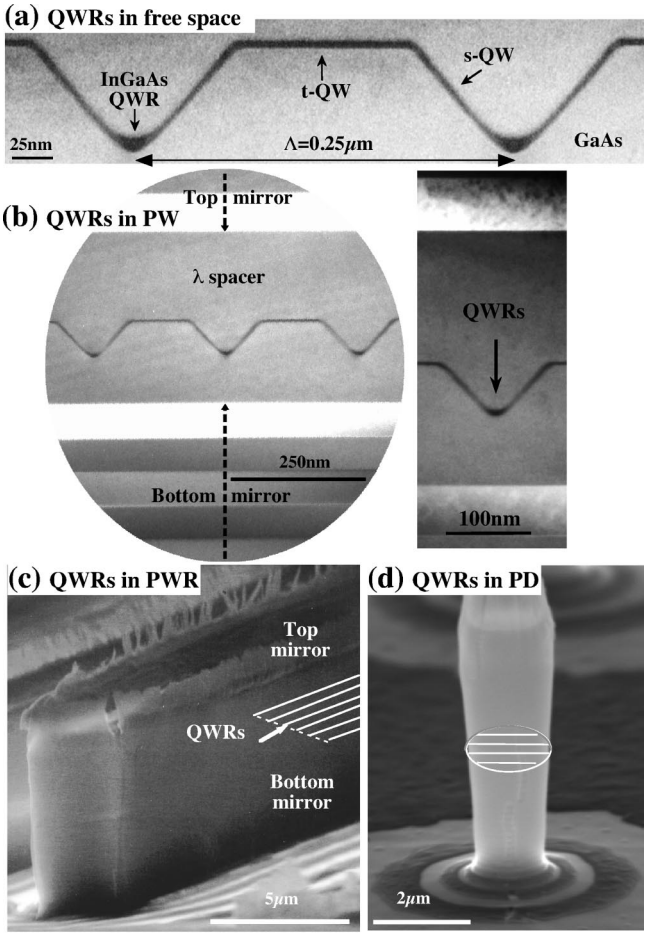

FIG. 1. Typical dark-field TEM cross sections of (a) a dense lateral array ($\Lambda = 0.25\ \mu$m) of $In_{0.15}Ga_{0.85}As/GaAs$ QWR's and (b) similar QWR's embedded in a $AlAs/Al_{0.07}Ga_{0.93}As$ λ planar Bragg microcavity; typical SEM overviews of similar QWR's in (c) a 2.8-μm-wide ridge microcavity and (d) a 1.6-μm-wide pillar microcavity.

been directly measured using electron energy-loss spectroscopy.[43,37] The nonuniform geometry and composition observed are expected to yield strong lateral confinement in these QWR's.

A typical TEM cross section of similar QWR's embedded in a λ planar Bragg microcavity is presented in (b), together with a magnified view. The array of QWR's, identical to the free space array above, is located in between the bottom and top Bragg mirrors. Fast planarization of the GaAs growth front after the wires occurred before the deposition of the top mirror that exhibits perfectly flat interfaces. The resulting spacer size $\lambda \sim 250$ nm is the smallest achieved with QWR's inside.[31,32] In spite of the regrowth process, high structural quality is achieved, as evidenced by the absence of any signature of the regrown interface or other defects in the image. Note that all thicknesses and contents were designed to yield spatial and spectral resonant coupling between the QWR's and the microcavity at low temperature.

Typical SEM cross sections of $\sim$micron-wide ridge and pillar resonators processed from the planar microcavity are depicted in (c) and (d), respectively. The images highlight the quality of the top surface of the cavity and the smoothness of their sidewalls (no visible fluctuations). Aside from a slight ($<0.2\ \mu$m) underetching at the top of the structures, very straight etched sidewalls are obtained, in spite of the large aspect ratio of the structures (1:6), which required fine optimization of the RIE process used to pattern the structures.[44] Note that the filamentary layers on top of the structures are photoresist remnants that are strongly hardened during the RIE process. The high structural quality of all structures described above is essential to minimize optical scattering and diffraction at the different interfaces, which would otherwise introduce additional losses that would reduce the finesse of the different microcavities.

III. ONE-DIMENSIONAL PROPERTIES OF QUANTUM WIRES IN FREE SPACE

We provide here unambiguous evidences of strong lateral quantization effects in the optical spectra of QWR's in free space. We use for that purpose a combination of conventional PL and PL excitation techniques in order to observe higher lateral subbands and transitions, which directly demonstrates the existence of several quantum confined states.

A. Experimental setup

The measurements were performed in a pseudobackscattering geometry from the (100) plane, using light from a tunable Ti:sapphire laser pumped by an all-solid diode pumped laser at 532 nm. The excitation light was focused onto a spot $\approx 30\ \mu$m in diameter, with power densities of about 5 W/cm^2, on the surface of the samples maintained at 15 K inside a helium-flow cryostat. The emitted light was dispersed by a 1000-mm double grating spectrometer and detected by a nitrogen-cooled Ge photodiode and standard lock-in techniques. The spectral resolution was fixed at 0.6 meV.

B. Photoluminescence spectroscopy

We provide in the inset of Fig. 2(a) the low-temperature (15 K) and low excitation power (5 W/cm^2) PL spectrum (dashed line) of a typical $In_{0.15}Ga_{0.85}As/GaAs$ QWR structure with a vertical effective thickness of 10 nm. The peak at 1.366 eV originates from the QWR's in the bottom of the grooves, whereas the peak at 1.390 eV comes from the *t*-QW's on the (100) facet connecting the grooves together, as confirmed by cathodoluminescence imaging at the corresponding emission energy of similar structures.[45] Quite remarkably, the emission from the QWR's is as intense as that from the *t*-QW's in spite of their much smaller active volume, thanks to efficient carrier capture into the wires. The QWR emission line is symmetric and displays a very narrow linewidth of 5.5 meV, evidencing the high uniformity between the wires over the probed area ($\sim 30\ \mu$m corresponding to about $\approx$120 wires).

The PL excitation spectrum detected at the QWR transition energy (solid line) exhibits a single series of five, well-defined peaks attributed to excitonic resonances associated with transitions between 1D subbands. The spectrum is fully

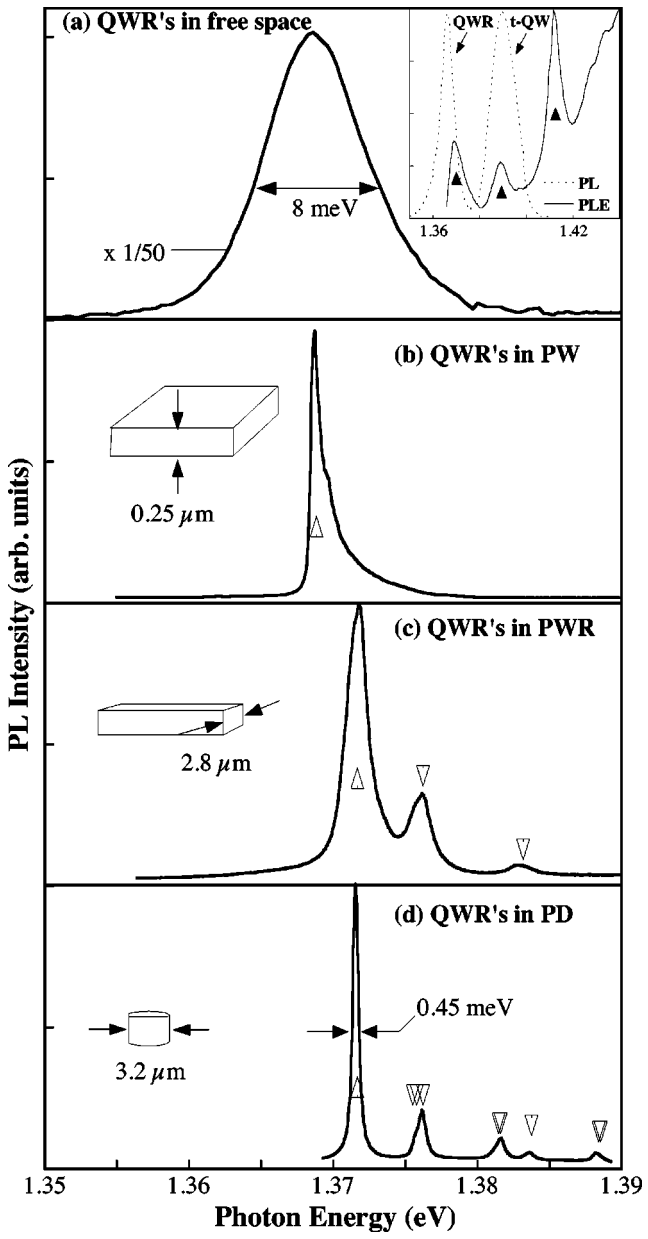

FIG. 2. Inset: PL (dashed line) and PL excitation (solid line) spectra of a 10-nm-thick $In_{0.15}Ga_{0.85}As/GaAs$ QWR array. Normalized μPL spectra of InGaAs QWR's: (a) in free space and (b,c,d) embedded: (b) in a PW, (c) in a 2.8-μm-wide PWR, (d) in a 3.2-μm-wide PD, at resonance; the open triangles are the calculated cavity mode energies. The temperature is 15 K.

dominated by excitonic effects thanks to the dominant role of Coulomb correlations in 1D systems leading to a vanishing Sommerfeld factor.[12,10] The very sharp linewidth (5.5 meV) together with a remarkably small Stokes shift (3 meV) of the first transition confirms the high uniformity achieved. The considerable energy separation between the ground-state and first-excited-state transitions of 20 meV, of the order of the thermal energy at room temperature, evidences strong lateral confinement. Such strong confinement has been observed over a large range of thickness and was traced back to the In enrichment at the center of the wires.[14]

IV. EFFECTS OF PHOTON DIMENSIONALITY ON EMISSION PROPERTIES

The complete control over the photon dimensionality in our structures allows us to systematically characterize the modifications in the QWR emission properties induced by the PW, PWR, and PD in the spectral, spatial, temporal, and polarization domains. We use for that purpose a combination of energy-, angle-, time-, and polarization-resolved μPL techniques.

A. Experimental setup

The measurements were again performed in a pseudo-backscattering geometry from the (100) plane, using light at about 1.60 eV from the tunable Ti:sapphire laser, so as to excite carriers in the GaAs barrier only, below the stop band of the Bragg mirrors. An almost perfectly Gaussian excitation spot of ~ 2 μm was obtained by spectral and spatial filtering, and focusing on the sample surface with a microscope objective. The samples were measured between 15 and 100 K inside a helium-flow cryostat with a quartz optical window 8 mm in diameter and 200 μm in thickness, which ensures a minimum spot size. A computer driven piezoelectric motor adjusted the sample position using a feedback loop locked on a reference CCD image, hence correcting for any drift during measurements. The emission within a solid angle $\Omega = 0.16\pi$ (semiangle $\theta = 24°$) was dispersed by a 460 mm spectrograph and detected using a nitrogen-cooled CCD camera, yielding a spectral resolution of 0.1 meV. For angle-resolved measurements, the emission far-field pattern after the collection microscope objective was directly sent to the spectrograph in a parallel beam, and then dispersed and detected by the CCD camera. The resulting image thus contains both the spectral characteristics of the emission on one axis (calibrated in energy), and its spatial characteristics along the $[01\bar{1}]$ direction on the other axis (calibrated in emission angle in air or with the equivalent photon wave vector, both deduced from simple geometric arguments), with an angular resolution of $\sim 0.4°$. For time-resolved measurements, short pulses (3 ps) from the Ti:sapphire laser were used at a repetition rate of 76 MHz to excite the luminescence, which was detected by a microchannel plate coupled to a time-correlated photon counting unit, allowing for a time resolution better than 10 ps after instrumental deconvolution. For polarization-resolved measurements, we combined a linear polarizer with a half-wave plate polarization rotator in front of the spectrograph to prevent any influence of the grating direction on the detected intensity, and resolved the polarization parallel ($[01\bar{1}]$) and perpendicular ($[011]$) to the QWR axis.

B. Emission spectrum

1. Resonant coupling for decreasing photon dimensionality

We show in Figs. 2(a–d), the modifications in the 15-K normalized μPL spectra of $In_{0.15}Ga_{0.85}As/GaAs$ QWR's in microcavities of decreasing dimensionality at resonant coupling. A single emission peak centered at the reference QWR

emission energy at 1.366 eV is observed for the planar Bragg cavity in (b), with a strongly reduced linewidth ($\sim$1 meV; reduced by $\sim$1/10), a drastic increase of the on-axis intensity ($\sim\times 50$), and a high-energy tail as compared with free space spectrum in (a). The spectrum of QWR's in a 2.8-μm-wide ridge cavity in (c) exhibits a main peak, blueshifted by $\sim$3 meV with respect to the corresponding PL peak in the PW spectrum, as well as two weaker peaks on the high-energy side, respectively, separated by 4 and 7 meV. All peaks present a substantial high-energy tail. In the case of QWR's in a 3.2-μm-wide pillar cavity in (d), a series of very narrow (0.45 meV) lines of decreasing intensities are visible, separated by $\sim$5 meV and blueshifted with respect to the PW PL peak by $\sim$3 meV. All lines are highly symmetric in this case and do not present any high-energy tail.

2. Discussion

The increasingly rich QWR spectra with sharper features for decreasing cavity dimensionality observed above are interpreted in terms of the coupling between the excited carriers and the vacuum electromagnetic field, whose intensity and modal structure are cavity dependent. Considering a perturbative coupling in the dipole approximation, the SE rate associated with a broadened excitonic transition, Γ_x^{sp}, is given by Fermi's golden rule and reads[17]

$$\Gamma_x^{sp}=\int_0^{\infty}\left[\frac{2\pi}{\hbar}E_{vac}^2(\mathbf{r})|d_{x,0}|^2\rho^{ph}(\hbar\omega)\right]\mathcal{L}_x(\hbar\omega)d(\hbar\omega), \tag{1}$$

where $E_{vac}^2(\mathbf{r})$ is loosely referred to as the vacuum field intensity at position $\mathbf{r}$, $d_{x,0}$ is the excitonic optical matrix element, $\rho^{ph}(\hbar\omega)$ is the photon DOS, and $\mathcal{L}(\hbar\omega)$ is the final-state energy distribution of the excitonic transition. We reexpress the SE rate in a more convenient form to separate the different contributions:

$$\Gamma_x^{sp}=\int_0^{\infty}\left[\frac{2\pi}{\hbar}E_{vac}^2(\mathbf{r})|d|^2\sum_{\mathbf{k},|\mathbf{k}|=\omega/c}A(\mathbf{k})\rho^{ph}(\mathbf{k})\right]\times\mathcal{L}_x(\hbar\omega)d(\hbar\omega), \tag{2}$$

where $|d|$ is the optical matrix element without its angular dependence on the photon wave vector $\mathbf{k}$, which is taken into account in $A(\mathbf{k})$, while $\rho^{ph}(\mathbf{k})$ is the photon DOS in the $\mathbf{k}$ direction at the energy $\hbar\omega=\hbar kc$. Hence, the emission rate *at a particular energy and in a particular direction* in Eq. (2) depends on the availability of corresponding photon modes to which the emitter can couple, as well as on the intensity of the vacuum field at its position. The quantization of the photon wave vector $\mathbf{k}$ in microcavities leads to stronger resonances in the available photon modes at the quantized energies and directions, as well as to a larger concentration of the stationary vacuum field intensity at distinct antinodes, for microcavities confined in multiple dimensions.[1,16] As a consequence, in the PL spectra presented above, the emission is significantly enhanced when the QWR location and transition energy are resonant with such allowed cavity modes (CM's), at the expense of the emission into nonresonant modes at other energies and directions.

For QWR's in a PW in Fig. 2(b), the single peak observed corresponds to the fundamental longitudinal photon mode of the planar Bragg cavity, as deduced from the transfer-matrix calculation of the mode energy[46] [open triangle in (b)]. Due to the much larger free spectral range of the cavity as compared to the wire emission linewidth, higher-order longitudinal modes are not visible. The significant intensity enhancement ($\times 50$) results from the efficient collection of the highly directional mode pattern.[1,16] Moreover, the emission linewidth is now given by the narrow ($<$1 meV) CM linewidth, instead of the large spectral width related to the QWR inhomogeneous broadening (8 meV). The high-energy tail results from the partial collection of the continuum of modes at larger energies due to the mode dispersion in the confinement-free plane.

For QWR's in a PWR in Fig. 2(c), the additional lateral photon confinement is provided by the air-semiconductor reflection ($R\sim 0.30$), which is weaker than the vertical confinement brought about by the Bragg mirror reflections ($R\sim 0.99$) in this structure. In a separation-of-variables approach, this extra lateral confinement introduces a series of quantized transverse modes that are blueshifted with respect to the longitudinal mode of the PW. Indeed, the CM energies in the ridge cavity have been calculated using a perfectly reflecting planar mirror model,[20] and are in quantitative agreement with the observed peak positions in the μPL spectrum [open triangles in (c)]. The decreasing intensity for the peaks at higher energies is due to the larger detuning between the higher-order transverse photon modes and the wire emission, as well as their broader far-field pattern, which is less efficiently collected in the experiment. The photon modes still possess dispersion along the ridge axis, responsible for the high-energy tail observed for all peaks.

For QWR's in a PD in Fig. 2(d), the modes are confined in all directions (air-semiconductor confinement in the plane and Bragg mirror confinement in the normal direction) and are therefore fully discretized and dispersionless. The modes of the pillar cavity can be thought of as analogous to the discrete states of electronic QD's where the in-plane lateral confinement is weaker than the vertical confinement, resulting in a series of quantized transverse modes. The allowed CM's have been calculated taking into account the cylindrical geometry of the pillars, using the model developed in Ref. 27. This model treats the micropillar as a segmented optical waveguide whose confined mode in each layer is written as a simple linear combination of guided modes of a GaAs/air or AlAs/air optical waveguide. The calculated energies are again in excellent agreement with the observed peak positions in the μPL spectrum [open triangles in (d)]. Moreover, due to the dispersionless nature of the CM's, the peaks do not exhibit any high-energy tail and their linewidth ($\Delta\lambda<0.5$ meV) reflects the intrinsic cavity quality factor. Very large cavity quality factors, as large as $Q=\lambda/\Delta\lambda\sim 5000$, were inferred from pillar cavity modes as narrow as 0.28 meV; this high value was achieved in spite of the numerous fabrication steps involved. Among semiconductor microcavities, only microdisks were reported to exhibit

larger quality factors.[28] We note that the measured values of Q are limited by scattering losses rather than by absorption in our experiment, as a change in cavity mode linewidth when varying the pump intensity over five orders of magnitudes due to bleaching was not observed. In fact, writing the contribution of absorption losses as[47] $Q_{abs}=2\pi n_{eff}/\lambda\alpha_m$, where α_m is the modal absorption coefficient at the mode energy and n_{eff} is the effective refractive index , we can deduce an upper bound for the modal absorption in QWR's: $\alpha_m^{QWR} \ll 40\ \mathrm{cm}^{-1}$, which is smaller than in QW's [$\alpha_m^{QW} \sim 100$–$200\ \mathrm{cm}^{-1}$ (Ref. 47)].

In summary, the spectral and angular redistribution of the broad QWR emission into the available photon modes of low-loss strongly confining cavities is responsible for the increasingly rich and sharper structuring of the wire emission in the spectral domain for decreasing cavity dimensionality.

3. Size dependence of photon dot modal structure

The precise determination of the photon modal structure in pillar cavities is highly desirable for optimizing the performance of lasers based on such cavities.[33] It is however difficult to probe the sustained modes from outside, using reflectivity or transmission, as symmetry forbids the coupling with most of them.[27] Similar difficulties have also hindered the characterization of more complicated photonic crystals.[48] In the present case, we can probe the modal structure of the pillar cavities from inside, by investigating the emission of the embedded QWR's, used as an internal broadband light source feeding the different cavity modes.

In Fig. 3(a) we show the 15-K normalized μPL spectra of InGaAs/GaAs QWR's in pillars of different diameter between 4.8 and 1.1 μm. All spectra exhibit the usual set of sharp lines associated with the fully quantized photon modes of the PD's. The fundamental CM shows a pronounced shift to higher energies (28 meV) when decreasing the pillar diameter (from 1.371 eV at 4.8 μm to 1.399 eV at 1.1 μm). Simultaneously, the energy splitting between the modes increases notably from $\sim$2 meV to $\sim$18 meV. We also observe a broadening of the fundamental peak for diameters smaller than $\sim$2 μm, resulting in a degradation of Q down to $\sim$1700 for the narrowest pillar. We attribute the corresponding extra losses to light scattering at the etched sidewalls that scales with the pillar diameter,[49] rather than to an increase in QWR absorption at higher energies as in Ref. 21. Excellent agreement between the measured and calculated (triangles) cavity modes obtained with the model of Ref. 27 is achieved. A small deviation ($\sim$2 meV) is observed for the thinnest (1.1 μm) pillar only. We summarize in Fig. 3(b) the size dependence of the measured (symbols) and calculated (dashed lines) photon mode energies [the modes are labeled after the standard name of their ''parent'' guided modes, used in optical fibers[50] (EH and HE)]. This allows to unambiguously attribute the observed blueshift and the increased splitting between the cavity modes to photon confinement effects. We note that similar pillar cavities where only the top mirror was etched away exhibit a smaller mode separation than here (3.8 meV vs 6.3 meV for 2.6-μm pillars),[21] evidencing stronger confinement in our case. Similarities with the electron quantum confinement in QD's are obvious. However, quantization effects of similar magnitude are obtained for a lateral size two orders of magnitude larger in the case of PD's ($\sim$1 μm) than in QD's ($\sim$10 nm). This is due to the much larger extent of the photonic wave function as compared with the electronic wave function.

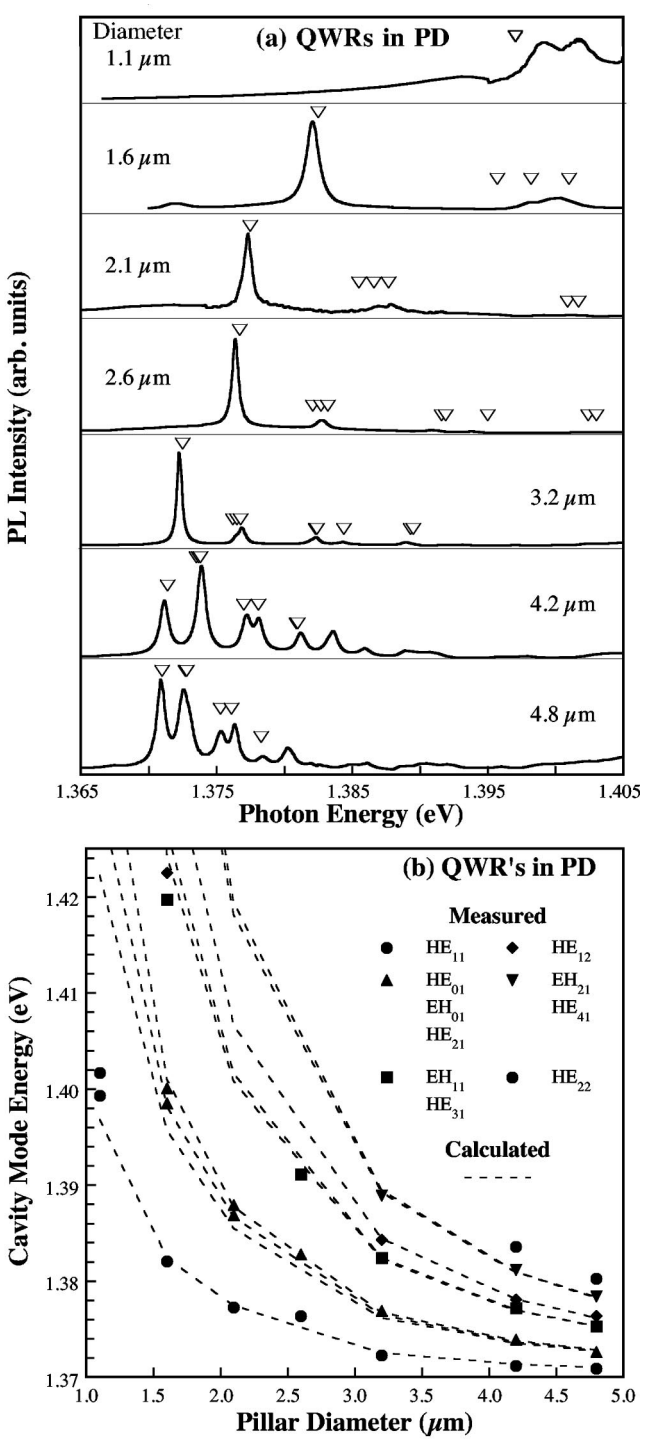

FIG. 3. (a) Normalized μPL spectra of InGaAs QWR's in PD's of different diameters between 4.8 and 1.1 μm measured at 15 K; empty triangles depict the calculated cavity mode energies. (b) Summary of the measured (closed symbols) and calculated (dashed lines) mode energies for the different diameters. The lines were drawn from a discrete set of calculated values.

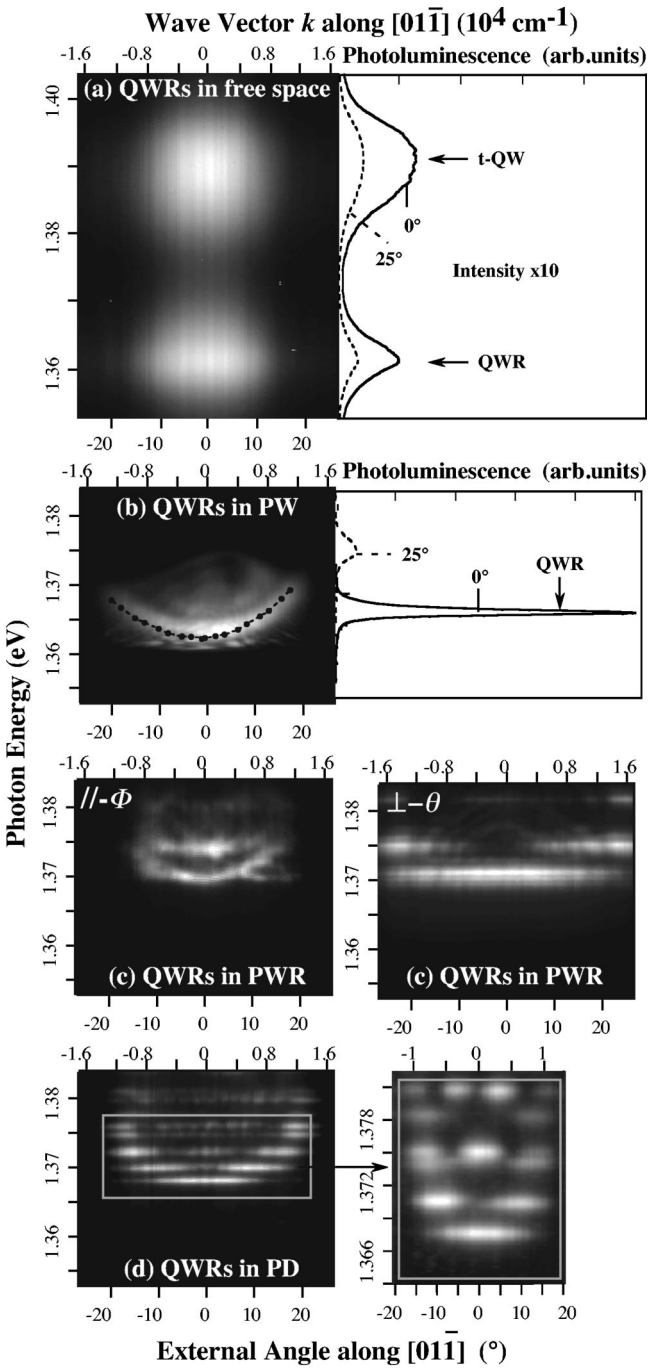

FIG. 4. CCD images of energy-dependent sections in the emission far-field pattern measured at 15 K for (a) InGaAs QWR's in free space, and (b) embedded in a PW, (c) in a 2.8-μm-wide PWR, (d) in a 4.8-μm-wide PD; PL spectra detected at 0° and 25° with respect to the sample normal are also shown for (a) and (b). The dotted line in (c) shows the calculated dispersion.

C. Emission pattern

1. Far field pattern for decreasing photon dimensionality

We demonstrate here the associated structuring of the emission pattern by resolving the angular dependence of the emission of QWR's in cavities. The CCD images in Figs. 4(a–d) display cross sections of the resonant QWR emission far-field pattern as a function of the energy for the different photon dimensionalities; the corresponding PL spectra at 0° and 25° with respect to the surface normal are also shown. In the case of QWR's in free space in (a), the emission is maximum at the *t*-QW and QWR peak energy and at the 0° normal direction, with a finite, broad spectral (~20 meV) and angular (>30°) spread, resulting in two featureless bright spots in the image. For QWR's in a planar Bragg cavity in (b), very bright emission is centered at the reference QWR energy (~1.364 eV) and 0° only, with a much narrower spectral (~2 meV) and angular (~10°) spread than in the free space case. It is accompanied at larger angles by a weaker emission continuously shifting to higher energies, resulting in a typical bright crescent in the image. In the case of QWR's in a 2.8 μm-wide ridge cavity in (c), two angle orientations are to be distinguished. For angles Φ parallel to the axis of the ridge, the image shows similar features as for the PW case with, however, two bright crescents visible at slightly higher energies at 1.370 and 1.374 eV. For angles θ perpendicular to the axis of the ridge, the features are quite different and the bright crescents are replaced by two narrow (~2 meV) emission bands at the same energies (1.370 and 1.374 eV) with maxima at, respectively, 0° and $\sim\pm 15°$. Features similar to the latter one are observed for QWR's in a 4.8-μm-wide pillar cavity in (d), with emission observed only at specific energies separated by ~3 meV and directions, resulting in a bright, dotlike pattern in the image.

2. Discussion

We interpret the CCD images with two different, but complementary, point of views. On one hand, we consider the angular distribution of the emission intensity, i.e., the emission pattern. On the other hand, we discuss them in terms of the allowed energies of the system in the reciprocal **k** space, i.e., the dispersion relation of the photonic system in the present weak-coupling regime.

QWR's in free space exhibit the weakly directional emission pattern of oriented dipoles, typical of heavy-hole-like transitions.[33] The emission of QWR's in microcavities mainly depends on the availability of photon modes at the corresponding energies and directions as already discussed in Sec. IV B 2 with the help of Eq. (2). The increasingly rich structuring of the emission pattern observed for decreasing cavity dimensionality is thus related to the photon modal structure in the different cavities, determining the resonances in their angular DOS $\rho^{ph}(\mathbf{k})$.

For QWR's in a PW in Fig. 4(b), the bright and narrow on-axis emission is a signature of the fundamental longitudinal mode of the planar Bragg cavity, whose highly directional lobe is efficiently collected.[1,16] Moreover, the mode dispersion in the cavity plane yields a continuum of quasimodes, whose emission patterns consist in concentric cones of larger apertures for increasing energies,[1,16] resulting in the continuous increase in emission energy observed for increasing angle in the image. In fact, the thus formed bright crescent is a direct measurement of the dispersion in the plane, as confirmed by the quantitative agreement obtained with the calculated dispersion determined by the transfer-matrix method[46] (dotted line). We note that due to the planar sym-

metry of the cavity, similar dispersion and sections in the emission pattern would be obtained in any other direction in the plane.

In the case of QWR's in a PWR in (c) and for angles Φ oriented parallel to the ridge, features similar to the PW case are not surprisingly observed in the CCD image, since we probe the photon confinement-free direction in this configuration. The extra lateral confinement however introduces a series of quantized transverse cavity modes that are blueshifted with respect to the longitudinal mode of the PW. Two such modes are indeed visible in the image, along with their dispersion along the ridge axis. For angles θ oriented perpendicular to the ridge axis, the CCD image displays completely different features and the emission pattern is anisotropic in the plane. In fact, we probe in this case the direction of photon confinement, as revealed by the absence of a mode dispersion, instead replaced by emission occuring only at the quantized energies and k vectors of the transverse modes.

Similarly, the CCD image of QWR's in a PD in (d) displays signatures of up to six fully confined and dispersionless transverse photon modes. We note that, in general, higher energy modes possess more maxima at larger angles, i.e., at equivalent k vectors. Such a far-field pattern in **k** space is related to the near-field electromagnetic distribution of the corresponding mode inside the pillar cavity via Fourier transforms.[20,51,50] In particular, the larger k components of the higher-order transverses modes indicate the expected modulated field distribution inside the pillar.[51] Such direct insight into the near field of confined photon states is to be contrasted with confined electronic states in nanostructures, whose direct observation is more difficult, due to the much smaller length scale ($\sim$10 nm).

In summary, the CCD imaging technique demonstrated here has allowed to observe systematic quantization of the cavity mode energy in the directions of photon confinement, and dispersive behavior in the free-propagation directions, resulting in an increasingly rich structuring of the emission pattern for decreasing cavity dimensionality. This technique holds a strong potential and should prove useful for probing the resonances of strongly coupled systems,[23] as well as for manipulating the reciprocal space with static or dynamic masks (liquid crystals, for instance) in order to select certain resonances of the system in emission or in absorption, for desired applications.

D. Emission dynamics

1. Emission rate for decreasing photon dimensionality

The redistribution of the QWR emission into the short-lived available cavity modes observed in the spectral and spatial domains above is also expected to modify their radiative lifetime and thus the SE rate, as originally predicted by Purcell.[52] This effect is evidenced here by looking at the characteristic times for the build up (τ_{rise}) and the decay (τ_{decay}) of the PL signal after short pulse excitation (3 ps). The approach used to determine such characteristic times from the PL temporal profile is illustrated in Fig. 5(a) for InGaAs/GaAs QWR's in a planar Bragg cavity at a temperature $T=60$ K and a carrier density $n=10^4$ e-h pairs per centimeter (dots). We consider the cascade decay of the carrier population among three discrete levels after optical excitation. The temporal evolution of the population of level 2, $n_2(t)$, yielding the PL signal, then reads in our case[53] (n_0 is the initial carrier population):

$$n_2(t)=n_0\frac{\tau_{decay}}{\tau_{rise}-\tau_{decay}}[e^{-t/\tau_{rise}}-e^{-t/\tau_{decay}}]. \qquad (3)$$

To extract τ_{rise} and τ_{decay}, we systematically convolute the instrumental response (dotted line) with the biexponential temporal evolution of the population $n_2(t)$ (dashed line), to obtain the best fit (solid line) to the data. Excellent agreement is indeed observed for a very fast rise time $\tau_{rise}=20$ ps and a much longer decay time $\tau_{decay}=600$ ps. Note that the convolution procedure used allows us to reach a resolution ($<$10 ps) well below the instrumental response ($\sim$60 ps). The SE rate enhancement of QWR's in microcavities is then evaluated by comparing τ_{decay} at the fundamental cavity mode energy for resonant coupling τ_{decay}^{in} with that at the same energy for nonresonant coupling, when the cavity mode lies at higher energy τ_{decay}^{out}, i.e., $\tau_{decay}^{out}/\tau_{decay}^{in}$. The identification of the SE rate enhancement with the ratio of decay times that is defined above assumes implicitly that the recombination is predominantly radiative and that the non-radiative lifetime is independent of the cavity detuning condition. At a temperature of 60 K, radiative recombination is the dominant process and, thus, this identification is justified. It is worth noting that thickness fluctuations across the sample are utilized to continuously tune the cavity mode energy with respect to the QWR emission energy.

We present in Figs. 5(b–d) the transient PL profiles obtained at $T=60$ K and $n=5\times10^4$ e-h pairs per centimeter in resonance (fat squares) and out of resonance (dots) for QWR's in microcavities of decreasing dimensionality: (b) in a planar Bragg cavity, (c) in a 2.8-μm-wide ridge cavity, and (d) in a 1.1-μm-wide pillar cavity. A systematic reduction in the QWR decay time is observed between the nonresonant and the resonant coupling case, yielding a steady increase of the SE rate enhancement from a mere $\times1.14\pm0.08$ value in the PW case, to $\times1.35$ for the PWR, on to a significant value of $\times1.68$ for the PD. We summarize in Fig. 6 the SE rate enhancement measured at different temperatures and carrier densities for cavities of different sizes. We deduce that the enhancement increases with decreasing dimensionality and lateral size; however, comparable values are obtained for ridge and pillar cavities of similar size. Moreover, an increase of either the temperature or the carrier density yields a slightly larger enhancement of the rate (e.g., from $\times1.46$ to $\sim\times1.70$ for the 1.1-μm-wide pillar).

2. Discussion

We again deduce from the SE rate expressed in Eq. (2) that the increasing spatial concentration of the vacuum field at particular positions and spectral concentration of the photon DOS at particular energies, for decreasing cavity dimensionality, are responsible for the observed rate enhancements when the QWR's and microcavities are resonantly coupled. In fact, evaluating the SE rate then merely reduces to mode

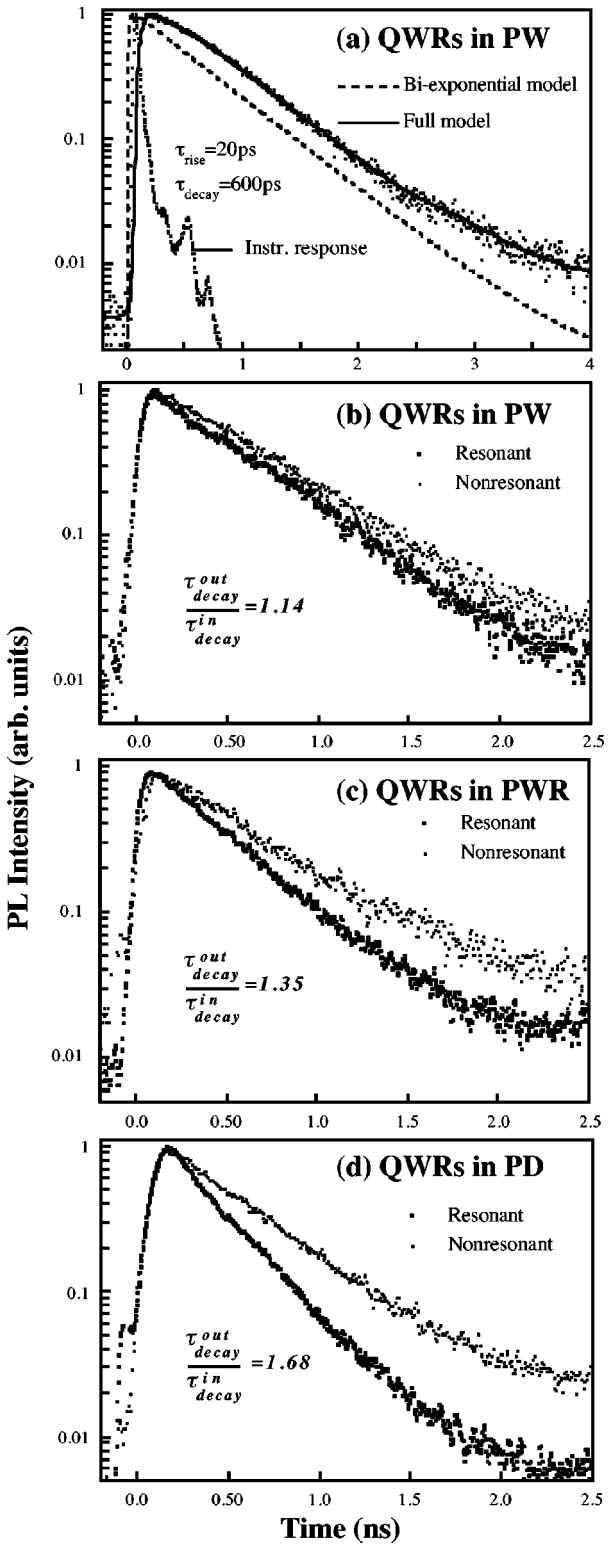

FIG. 5. (a) Transient PL of InGaAs QWR's in a PW at resonance obtained at 60 K; the calculated biexponential transient (dashed line) convoluted with the instrumental response (dotted line) yields the solid line showing excellent agreement with the measured transient. Transient PL of InGaAs QWR's (b) in a PW, (c) in a 2.8-μm-wide PWR, and (d) in a 1.1-μm-wide PD, measured in resonance (fat squares) and out of resonance (dots), at $T=60$ K and $n=5\times10^4$ *e-h* pairs/cm; the corresponding SE rate enhancements $\tau^{out}_{decay}/\tau^{in}_{decay}$ are also given.

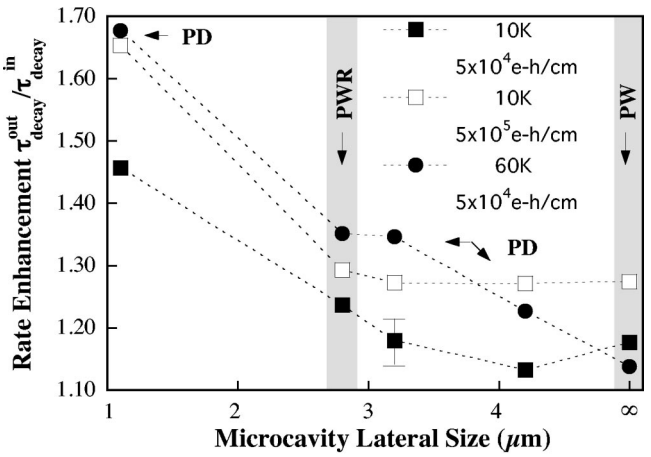

FIG. 6. Summary of the spontaneous emission rate enhancement $\tau^{out}_{decay}/\tau^{in}_{decay}$ of InAsGaAs QWR's in cavities of decreasing dimensionality and lateral size; values at two temperatures (10 and 60 K) and two carrier densities ($n=5\times10^4$ and 5×10^5 *e-h* pairs/cm) are presented.

counting in the reciprocal space, **k**, where the cavity modal structure is more easily visualized.[1,17]

Such calculations for planar Bragg cavities similar to ours showed that whereas the on-axis emission rate is strongly increased, the total rate is only weakly affected by the cavity ($\times1.2$),[54] in accordance with the weak total rate enhancement observed in Fig. 5(b) ($\times1.14$), while the on-axis intensity is strongly increased in Fig. 2(b) ($\times50$). Similar observations have been reported for QW's,[18] QD's,[26] and rare-earth atoms[55] in such cavities. Planar Bragg cavities are in fact limited in this context by a mode control over a small solid angle ($\Omega\ll4\pi$), such that the emitter can couple to numerous nonconfined leaky and guided modes.[54]

The introduction of lateral photon confinement yields mode control over a much wider solid angle, resulting in larger enhancements of the SE rate due to the strongly peaked DOS of PWR's and PD's.[1,16] A sizable rate enhancement is indeed observed in Fig. 5 for the 2.8-μm-wide ridge cavity ($\times1.35$) and for the 1.1-μm-wide pillar cavity ($\times1.68$). Note that this is the first evidence of SE rate enhancement entailed by a PWR, whereas previous reports exist for QW's and QD's in PD's.[22,56,30,26] We follow the approach undertaken in Ref. 30 to discuss quantitatively the amplitude of the observed enhancements. We first evaluate the Purcell factor associated with the fundamental mode of our pillars, $F_p=3Q(\lambda/n_r)^3/4\pi^2V_c$, where λ, n_r, V_c are, respectively, the emission wavelength, the effective refractive index, and the cavity volume, which gives the maximum obtainable rate enhancement. A steady increase $F_p\sim5$ to 25 is obtained when reducing the pillar diameter from 4.2 to 1.1 μm, although the corresponding quality factor decreases from $Q\sim5000$ to 1700, thanks to the faster decrease in V_c. A systematic larger rate enhancement for smaller pillars is indeed observed in Fig. 6, however of a much smaller amplitude than predicted. In fact, the coupling between the QWR's and the pillar cavity departs from an ideal situation as (i) the QWR emission linewidth $\Delta\omega_x$ is about an order of magnitude larger than the mode linewidth $\Delta\omega_c$, (ii) a small

energy detuning $\Delta E_{cav} \sim 5$ meV exists for the smallest pillar, (iii) the pillars contain about four QWR's that experience an averaged vacuum field smaller than its maximum value: $E_{mean}/E_{max} \sim 1/2$, (iv) the QWR's are coupled to several cavity modes, as the fundamental mode of such pillars are $g=2$ times degenerate,[44] and as leaky modes exhibiting a dynamics comparable to the free space case[30] are also present. The actual rate enhancement is then considerably reduced from the optimum value F_p and becomes[16,17]

$$\frac{\tau_{decay}^{out}}{\tau_{decay}^{in}} = gF_p \frac{\sqrt{\pi}\Delta\omega_c}{\Delta\omega_x} e^{-[2(\Delta E_{cav})/\Delta\hbar\omega_x]^2} \frac{|\mathbf{E}_{vac}(\mathbf{r})|^2}{|E_{max}|^2} + 1 \approx 1.6, \tag{4}$$

which is in fair agreement with the measured value ($\times 1.68$). Whereas the relatively weak rate enhancement is mainly limited by the QWR inhomogeneous broadening and by the spectral detuning with the cavity mode, we note that the orientation matching between the dipoles and the vacuum field is realized in QWR's. Moreover, whereas a similar rate enhancement was observed for QW's in pillar cavities,[56] the much narrower homogeneous linewidth of QD's has led to a larger rate enhancement of $\times 5$[30] to $\times 18$[28], although the QD locations and orientations were randomly distributed.

We briefly comment on the Purcell effect at the different temperatures and carrier densities reported in Fig. 6. A reduction in the Purcell effect could be anticipated for increasing temperature or density, due to an increase in the emission linewidth, or, in other words, of the carrier population at energies different than the cavity mode energy. In contrast, a slight increase is observed in the experiments, although the occurence of stimulated emission is most unlikely as the emitted intensity varies linearly with the excitation power. The interpretation may lie beyond the approximation of localized excitons used here (noninteracting dipoles), by taking into account the carrier population kinetics, as suggested in previous works.[57,58]

In summary, increasing SE rate enhancement has been demonstrated for decreasing cavity dimensionality and size. In contrast to the significant cavity effects obseved in the spectral and spatial domains, photon confinement in at least two directions in PWR's and PD's is necessary to obtain peaked singularities in the photon DOS and thus induce significant changes in the time domain.

3. Photon dot as a probe of carrier diffusion

In this section, we use the finite lateral size of ridge and pillar cavities as a passive experimental tool to get insight into the real-space diffusion of hot carriers in QWR's following short pulse excitation. In Fig. 7(a) we present the transient PL profiles of QWR's in a 2.8-μm-wide ridge, for nonresonant coupling and at 100 K. Interestingly, τ_{decay} is shortened from 390 to 200 ps when changing the orientation of the ridge from parallel to perpendicular to the QWR axis. In fact, when the photogenerated carriers diffusing along the QWR's reach the ridge sidewalls, an additional nonradiative recombination channel opens up with a rate $1/\tau^{walls}$, therefore shortening the total decay time. In other words, the cavity walls actually act as carrier diffusion markers in transient PL measurements, allowing for the estimation of the diffusion length L_{diff}.

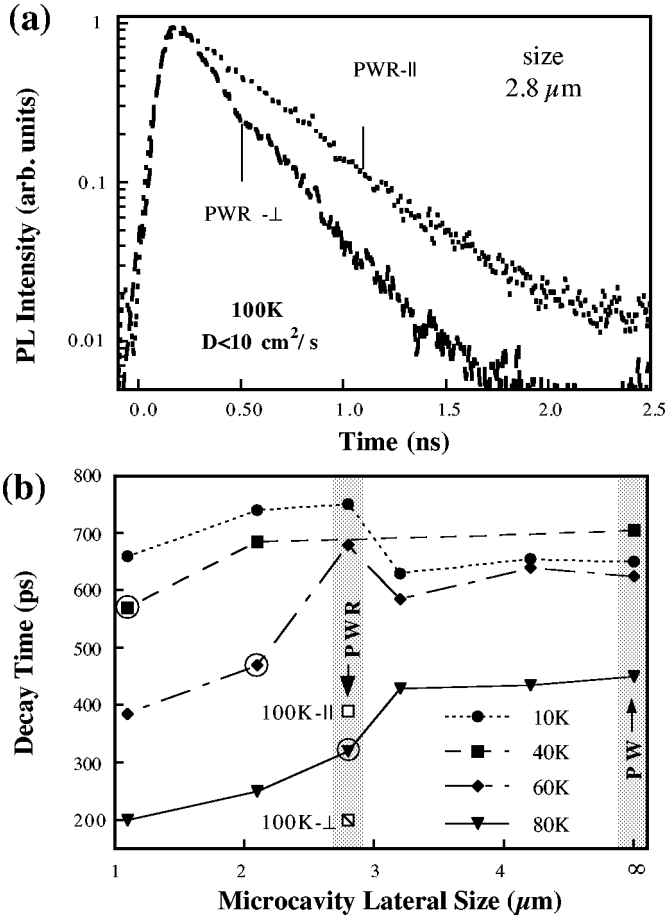

FIG. 7. (a) Transient PL profiles of InGaAs QWR's in a 2.8-μm-wide PWR, measured out of resonance at 100 K, and for an orientation of the PWR either parallel or perpendicular to the QWR axis. (b) Summary of the decay times τ_{decay} as a function of the cavity lateral size for the different temperatures.

We present in Fig. 7(b) the measured τ_{decay} as a function of the lateral size of the pillar cavities d and of the temperature. The decay time is found to drop for sufficiently small lateral sizes, which allows a rough estimate of $L_{diff} \approx d/2$ at the drop. We deduce $L_{diff} < 0.5$ μm at 10 K, $L_{diff} \sim 0.5$, 1, and 1.5 μm at 40, 60, and 80 K, respectively, in accordance with the usual mobility increase in this temperature range.[59] The measured temperature dependence of L_{diff} agrees well with that obtained by the time-of-flight method for similar lattice-matched V-QWR's.[60] Moreover, in the present case of rather wide cavities and low carrier diffusivities D, the sidewall recombination rate and the diffusivity are related by $\tau^{walls} = d^2/\pi^2 D$.[61] After extracting τ^{walls} from the measured decay times, we thus determine the following upper bound values for the diffusivity obtained from the results on 1.1-μm-wide pillars: $D \sim 0$ cm^2/s at 10 K, and $D < 0.3$, 1, 3, and 10 cm^2/s at 40, 60, 80, and 100 K, respectively. The rather small values of the diffusivity obtained at low temperature ($D \sim 0$ cm^2/s at 10 K) corroborates other optical studies, which have evidenced the role of disorder in this

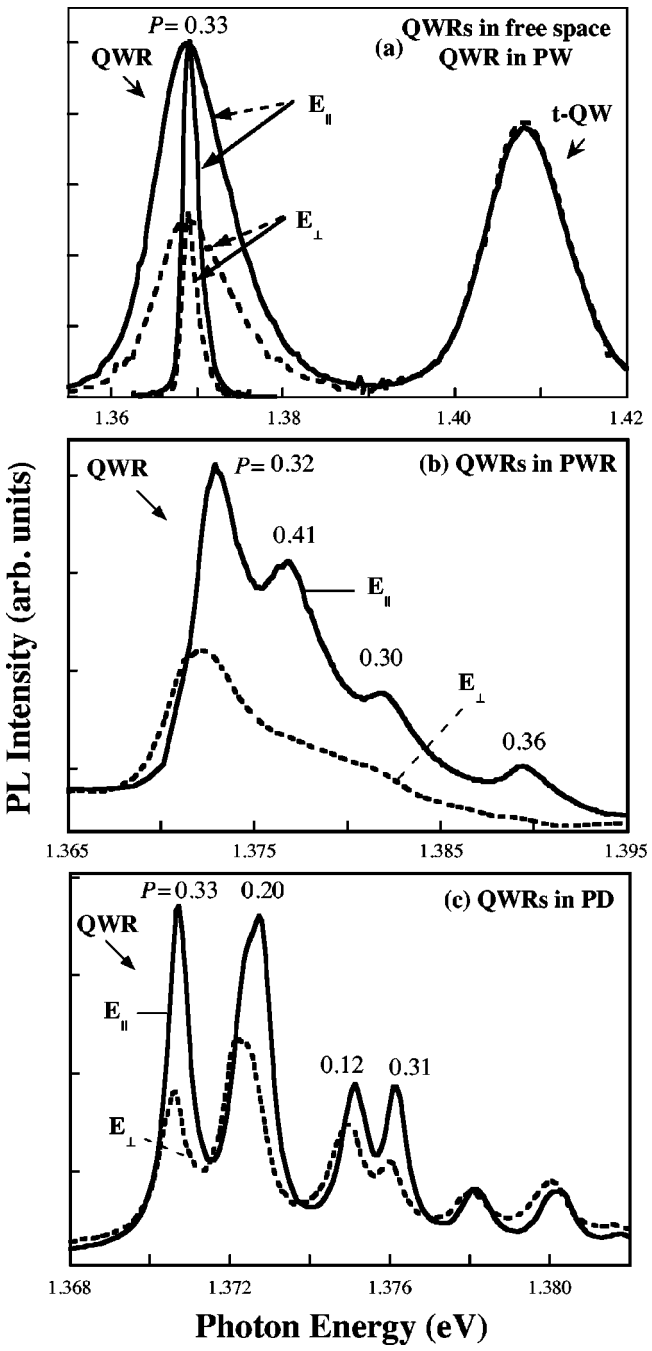

FIG. 8. PL spectra of InGaAs QWR's at 15 K (a) in free space and in a PW, (b) in a 2.8-μm-wide PWR, (c) in a 4.8-μm-wide PD. Emission is decomposed into linearly polarized light parallel ($E_{||}$, solid lines) or perpendicular ($E_{\perp}$, dashed lines) to the QWR axis.

temperature range.[13,60] Optical studies of diffusivity in quantum wells also concluded that interface roughness reduces drastically the diffusion of excitons at low temperature in narrow quantum wells.[62]

E. Emission polarization

The dependence of the PL spectra on the linear polarization parallel (solid lines) or perpendicular (dashed lines) to the wire axis is depicted in Figs. 8(a–c) for QWR's in cavities of decreasing dimensionality. A striking anisotropy yielding a degree of polarization of 0.33 in favor of the parallel configuration is observed in the free space case in (a). Such anisotropy was found to originate both from the presence of lateral confinement and triaxial strain in the QWR's.[14] The exact same anisotropy is observed in the planar Bragg cavity case in (a), which is not surprising as a PW is perfectly symmetric in the plane and has therefore no polarization selection mechanism. The parallel polarization is also favored in case of a 2.8-μm-wide ridge cavity in (b), and of a 4.8-μm-wide pillar cavity in (c), with a degree that however slightly depends on the considered cavity mode. In these cases, a specific orientation of the electric field is in general associated with a cavity mode[50] and the anisotropy is then determined by the coupling with the QWR dipole. For instance, as the electric field associated with the fundamental mode of the pillar cavity (HE_{11}) has a main transverse component in the plane of the wire without a favored orientation,[50,44] the intrinsic QWR anisotropy remains unchanged. In contrast, the weaker anisotropy of the second ($P=0.20$) and third ($P=0.12$) PL peak may be related to the associated modes (EH_{01} and EH_{11}, respectively) that possess a main component normal to the wires, resulting in a weaker coupling that alters the intrinsic QWR anisotropy. Such polarization selection mechanisms are of prime importance for locking the polarization state of VCSEL's, and therefore reduce their noise characteristics and response time.[32]

V. CONCLUSION

State-of-the-art strained QWR's embedded in high finesse, multidimensional Bragg-air microcavities allowed us to investigate the coupling between 1D carriers and 3D, 2D, 1D, and 0D photon states. We could, in particular, elucidate in a systematic way the impact of the cavity dimensionality on the QWR spontaneous emission in the spectral, spatial, temporal, and polarization domains using different micro-PL techniques. Larger effects were demonstrated for resonant cavities confining in multiple dimensions and of smaller sizes. We observed in particular, sharp (0.28 meV), intense ($\times 50$), and directional emission at an enhanced rate ($\times 1.7$) in the case of fully confined PD's. The cavity effects above were interpreted in terms of a redistribution of the QWR emission into resonances in the distribution of photon modes induced by the confinement in the weak-coupling limit. Moreover, these resonances were directly visualized in the reciprocal space exhibiting systematic wave-vector quantization in the directions of photon confinement, and dispersive behavior in the free propagation directions, in close agreement with model calculations.

ACKNOWLEDGMENTS

We wish to thank A. Rudra for the epitaxial growth of the samples, E. Costard for carrying out the RIE process, K. Leifer for providing the TEM micrographs, F. Lelarge and R. Houdre for fruitful discussions. This work was supported by the Swiss Priority Program Optics II.

[1] *Confined Electrons and Photons: New Physics and Applications*, Vol. 340 of *NATO Advanced Studies Institute, Series B: Physics*, edited by E. Burstein and C. Weisbuch (Plenum Press, London, 1995).
[2] P. Harrison, *Quantum Wells, Wires and Dots, Theoretical and Computational Physics* (Wiley, New York, 2000).
[3] C. Weisbuch and B. Vinter, *Quantum Semiconductor Structures* (Academic Press, Boston, 1991).
[4] H. Akiyama, J. Phys.: Condens. Matter **10**, 3095 (1998).
[5] R. Cingolani and R. Rinaldi, Nuovo Cimento D **16**, 1 (1993).
[6] D. Bimberg, M. Grundmann, and N. N. Ledentsov, *Quantum Dot Heterostructures* (Wiley, New York, 1999).
[7] Y. Arakawa and H. Sakaki, Appl. Phys. Lett. **40**, 939 (1982).
[8] S. Schmitt-Rink, D. S. Chemla, and D. A. B. Miller, Adv. Phys. **38**, 89 (1989).
[9] U. Bockelmann and G. Bastard, Phys. Rev. B **45**, 1688 (1992).
[10] F. Rossi and E. Molinari, Phys. Rev. Lett. **76**, 3642 (1996).
[11] F. Rossi, G. Goldoni, and E. Molinari, Phys. Rev. Lett. **78**, 3527 (1997).
[12] T. Ogawa and T. Takagahara, Phys. Rev. B **44**, 8138 (1991).
[13] F. Vouilloz, D. Y. Oberli, M. A. Dupertuis, A. Gustafsson, F. Reinhardt, and E. Kapon, Phys. Rev. B **57**, 12 378 (1998).
[14] C. Constantin, E. Martinet, F. Lelarge, K. Leifer, A. Rudra, and E. Kapon, J. Appl. Phys. **88**, 141 (2000).
[15] G. Biasiol and E. Kapon, Phys. Rev. Lett. **81**, 2962 (1998).
[16] *Confined Photon Systems: Fundamentals and Applications*, Lecture Notes in Physics, edited by H. Benisty, C. Weisbuch, J. M. Gerard, R. Houdre, and J. Rarity (Springer-Verlag, Berlin, 1999).
[17] *Spontaneous Emission and Laser Oscillation in Microcavities*, edited by H. Yokoyama and K. Ujihara (CRC Press, Boca Raton, 1995).
[18] K. Tanaka, T. Nakamura, W. Takamatsu, M. Yamanishi, Y. Lee, and T. Ishihara, Phys. Rev. Lett. **74**, 3380 (1995).
[19] L. Dae Ho, Y. Gye Mo, and L. Kee Young, J. Appl. Phys. **83**, 2282 (1998).
[20] A. Kuther, M. Bayer, T. Gutbrod, A. Forchel, P. A. Knipp, T. L. Reinecke, and R. Werner, Phys. Rev. B **58**, 15 744 (1998).
[21] J. P. Reithmaier, M. Rohner, H. Zull, F. Schafer, A. Forchel, P. A. Knipp, and T. L. Reinecke, Phys. Rev. Lett. **78**, 378 (1997).
[22] B. Ohnesorge, M. Bayer, A. Forchel, J. P. Reithmaier, N. A. Gippius, and S. G. Tikhodeev, Phys. Rev. B **56**, R4367 (1997).
[23] R. Houdre, C. Weisbuch, R. P. Stanley, U. Oesterle, P. Pellandini, and M. Ilegems, Phys. Rev. Lett. **73**, 2043 (1994).
[24] A. I. Tartakovskii, V. D. Kulakovskii, A. Forchel, and J. P. Reithmaier, Phys. Rev. B **57**, R6807 (1998).
[25] J. Bloch, R. Planel, V. Thierry-Mieg, J. M. Gerard, D. Barrier, J. Y. Marzin, and E. Costard, Superlattices Microstruct. **22**, 371 (1997).
[26] L. A. Graham, D. L. Huffaker, Q. Deng, and D. G. Deppe, Appl. Phys. Lett. **72**, 1670 (1998).
[27] J. M. Gerard, D. Barrier, J. Y. Marzin, R. Kuszeleqicz, L. Manin, E. Costard, V. Thierry-Mieg, and T. Rivera, Appl. Phys. Lett. **69**, 449 (1996).
[28] B. Gayral, J. M. Gerard, A. Lemaitre, C. Dupuis, L. Manin, and J. L. Pelouard, Appl. Phys. Lett. **75**, 1908 (1999).
[29] L. A. Graham, D. L. Huffaker, and D. G. Deppe, Appl. Phys. Lett. **74**, 2408 (1999).
[30] J. M. Gerard, B. Sermage, B. Gayral, B. Legrand, E. Costard, and V. Thierry-Mieg, Phys. Rev. Lett. **81**, 1110 (1998).
[31] T. Arakawa, M. Nishioka, Y. Nagamune, and Y. Arakawa, Appl. Phys. Lett. **64**, 2200 (1994).
[32] A. Chavez Pirson, H. Ando, H. Saito, and H. Kanbe, Appl. Phys. Lett. **64**, 1759 (1994).
[33] T. Baba, T. Hamano, F. Koyama, and K. Iga, IEEE J. Quantum Electron. **28**, 1310 (1992).
[34] A. V. Kavokin, M. A. Kaliteevski, and M. R. Vladimirova, Phys. Rev. B **54**, 1490 (1996).
[35] F. Tassone and F. Bassani, Phys. Rev. B **51**, 16 973 (1995).
[36] M. A. Kaliteevski, S. Brand, R. A. Abram, V. V. Nikolaev, M. V. Maximov, N. N. Ledenstov, C. Sotomayor-Torres, and A. V. Kavokin, Phys. Rev. B **61**, 13 791 (2000).
[37] F. Lelarge, C. Constantin, K. Leifer, A. Condo, V. Iakovlev, E. Martinet, A. Rudra, and E. Kapon, Appl. Phys. Lett. **75**, 3300 (1999).
[38] F. Lelarge, C. Priester, C. Constantin, A. Rudra, K. Leifer, and E. Kapon, Appl. Surf. Sci. **166**, 290 (2000).
[39] C. Constantin, E. Martinet, A. Rudra, K. Leifer, F. Lelarge, G. Biasiol, and E. Kapon, J. Cryst. Growth **207**, 161 (1999).
[40] C. Constantin, E. Martinet, A. Rudra, and E. Kapon, Phys. Rev. B **59**, R7809 (1999).
[41] C. Constantin, E. Martinet, B. Gayral, J. M. Gerard, K. Leifer, A. Rudra, F. Lelarge, and E. Kapon, Mater. Sci. Eng., B **74**, 158 (2000).
[42] A. Condo, K. Leifer, A. Rudra, J. Michler, E. Blank, and E. Kapon, *Microscopy of Semiconducting Materials* (IOP, Oxford, 2000).
[43] K. Leifer, A. Rudra, G. Biasiol, J. Michler, E. Blank, P. A. Buffat, and E. Kapon, *Microscopy of Semiconducting Materials* (IOP, Oxford, 1999).
[44] B. Gayral, J. M. Gerard, B. Legrand, E. Costard, and V. Thierry-Mieg, Appl. Phys. Lett. **72**, 1421 (1998).
[45] A. Gustafsson, L. Samuelson, J. O. Malm, G. Vermeire, and P. Demeester, Appl. Phys. Lett. **64**, 695 (1994).
[46] P. Yeh, *Optical Waves in Layered Media* (Wiley, New York, 1988).
[47] R. E. Slusher, A. F. J. Levi, U. Mohideen, S. L. McCall, S. J. Pearton, and R. A. Logan, Appl. Phys. Lett. **63**, 1310 (1993).
[48] D. Labilloy, H. Benisty, C. Weisbuch, T. F. Krauss, R. M. De La Rue, V. Bardinal, R. Houdre, U. Oesterle, D. Cassagne, and C. Jouanin, Phys. Rev. Lett. **79**, 4147 (1997).
[49] T. Rivera, J. P. Debray, J. M. Gerard, B. Legrand, C. L. Manin Ferlazzo, and J. L. Oudar, Appl. Phys. Lett. **74**, 911 (1999).
[50] A. Yariv, *Optical Electronics, Optics Letters* (Saunders College, San Francisco, 1991).
[51] T. Gutbrod, M. Bayer, A. Forchel, P. A. Knipp, T. L. Reinecke, A. Tartakovskii, V. D. Kulakovskii, N. A. Gippius, and S. G. Tikhodeev, Phys. Rev. B **59**, 2223 (1999).
[52] E. M. Purcell, Phys. Rev. **69**, 681 (1946).
[53] G. Bastard, *Wave Mechanics Applied to Semiconductor Heterostructures* (Edition de Physique, Les Ulis, France, 1988).
[54] C. C. Lin, D. G. Deppe, and C. Lei, IEEE J. Quantum Electron. **30**, 2304 (1994).
[55] A. M. Vredenberg, N. E. J. Hunt, E. F. Schubert, D. C. Jacobson, J. M. Poate, and G. J. Zydzik, Phys. Rev. Lett. **71**, 517 (1993).
[56] T. Tezuka, S. Nunoue, H. Yoshida, and T. Noda, Jpn. J. Appl. Phys., Part 2 **2**, L54 (1993).
[57] Y. Hanamaki, H. Kinoshita, H. Akiyama, N. Ogasawara, and Y.

Shiraki, Phys. Rev. B **56**, R4379 (1997).
[58] *Microcavities and Photonic Bandgaps: Physics and Applications*, Vol. 324 of *NATO Advanced Studies Institute, Series E: Applied Sciences*, edited by R. Rarity and C. Weisbuch (Kluwer Academic, Dordrecht, 1996).
[59] P. Y. Yu and M. Cardona, *Fundamentals of Semiconductors* (Springer-Verlag, Berlin, 1996).
[60] F. Vouilloz, Ph.D. thesis, Swiss Federal Institute of Technology, 1998.
[61] G. Mayer, B. E. Maile, R. Germann, A. Forchel, P. Grambow, and H. P. Meier, Appl. Phys. Lett. **56**, 2016 (1990).
[62] H. Hillmer, A. Forchel, S. Hansmann, M. Morohashi, E. Lopez, H. P. Meier, and K. Ploog, Phys. Rev. B **39**, 10 901 (1989).